

Grain growth and superconductivity of rhenium electrodeposited from water-in-salt electrolytes

Cite as: J. Appl. Phys. **127**, 085301 (2020); <https://doi.org/10.1063/1.5139909>

Submitted: 25 November 2019 . Accepted: 10 February 2020 . Published Online: 25 February 2020

William D. Sides , Ehsan Hassani, David P. Pappas, Yang Hu , Tae-Sik Oh , and Qiang Huang 



View Online



Export Citation



CrossMark

ARTICLES YOU MAY BE INTERESTED IN

[The effect of Co-doping on dielectric properties and bandgap of zinc silicate nanowires](#)

Journal of Applied Physics **127**, 085104 (2020); <https://doi.org/10.1063/1.5121616>

[Raman evidence for absence of phase transitions in negative differential resistance thin film devices of niobium dioxide](#)

Journal of Applied Physics **127**, 084503 (2020); <https://doi.org/10.1063/1.5140543>

[Numerical simulation and validation of subsurface modification and crack formation induced by nanosecond-pulsed laser processing in monocrystalline silicon](#)

Journal of Applied Physics **127**, 085106 (2020); <https://doi.org/10.1063/1.5130701>

Lock-in Amplifiers
up to 600 MHz



Grain growth and superconductivity of rhenium electrodeposited from water-in-salt electrolytes

Cite as: J. Appl. Phys. 127, 085301 (2020); doi: 10.1063/1.5139909

Submitted: 25 November 2019 · Accepted: 10 February 2020 ·

Published Online: 25 February 2020



View Online



Export Citation



CrossMark

William D. Sides,¹  Ehsan Hassani,² David P. Pappas,³ Yang Hu,¹  Tae-Sik Oh,²  and Qiang Huang^{1,a)} 

AFFILIATIONS

¹Department of Chemical and Biological Engineering, University of Alabama, Tuscaloosa, Alabama 35487, USA

²Department of Chemical Engineering, Auburn University, Auburn, Alabama 36849, USA

³National Institute of Standards and Technology, Boulder, Colorado 80305, USA

^{a)}Author to whom correspondence should be addressed: qhuang@eng.ua.edu

ABSTRACT

The relationship between superconductivity and the film preparation conditions, i.e., the thickness and annealing process, in electrodeposited rhenium (Re) films is studied in order to understand the effect of grain size and impurities on the film's superconducting transition temperature, T_c . A water-in-salt electrolyte was used to mitigate embrittlement by reducing hydrogen evolution at the cathode where Re is deposited. The as-deposited films exhibit a highly disordered atomic structure and superconductivity up to a temperature of $T_c > 5.8$ K, consistent with that expected from amorphous films. A reduction of the critical temperature of superconductivity is found to accompany grain growth. However, for film thicknesses less than 300 nm the grain growth is inhibited. This leads to a retention of the critical temperature upon annealing these thin films. A reduction of impurities in Re films is found to accompany annealing, and significant grain growth is found to proceed rapidly at temperatures of 220 °C in inert atmospheres. The introduction of hydrogen in the annealing ambient further facilitates this grain growth.

<https://doi.org/10.1063/1.5139909>

I. INTRODUCTION

Low temperature superconducting materials are becoming increasingly important in the electronics industry, particularly as quantum computing is scaled to higher qubit counts and as Josephson-junction based devices continue to be explored. These devices require superconducting materials for circuits, and quantum computing systems additionally require superconducting materials to eliminate ohmic heating so that thermal perturbation may be avoided and sub-kelvin temperatures may be more sustainable within the operating environment. Additionally, materials with a superconducting critical temperature (T_c) at least 3 K, the base temperature of typical cryocoolers, and preferably above 4.2 K, the boiling point of liquid helium, become practical for a much wider set of uses in the scientific, industrial, and medical applications. Currently, superconductors made of niobium or its alloys with Sn or Ti are most commonly used; however, they are prone to oxidation and difficult to solder. Fabrication is typically performed either by billet extrusion and drawing for wiring or by vacuum deposition methods for microdevices.¹ On the other hand, the superconducting metal rhenium can be much more convenient to work with. It is ductile and can be soldered or ultrasonically

wire-bonded. The relatively high melting point of Re, 3186 °C, suggests a high resistance to electromigration and reliability in circuitry.² In addition, Re does not easily interdiffuse into many other metals common in circuitry.^{3,4} Finally, Re can be electrodeposited from aqueous solutions—a process compatible with other electronics fabrication processes—and the resulting films have enhanced T_c of nearly 6 K,^{5,6} well above the intrinsic T_c of Re metal, 1.7 K. This enhancement is in line with that of amorphous Re films prepared by e-beam evaporation onto cooled substrates and other amorphous transition metal films.⁷ The enhancement of T_c observed in the electroplated films is important for several reasons. First, it is well above the boiling point of helium. Combined with its compatibility with electroplated Au and Cu, this opens up a new method for fabricating low-cost superconducting circuit boards and components for detectors and electronics that operate at 4 K. Second, the stability of T_c in the electrodeposited films at room temperature is in stark contrast with the irreversible changes in the e-beamed films tested by Collver. In the present films, we show that it is possible to maintain enhanced T_c 's in the electrodeposited films for significantly higher annealing temperatures, opening the possibility of incorporation of these films into multi-layer circuit boards.

The electrodeposition of Re occurs at a significant overpotential to hydrogen evolution. Hydrogen bubbles continuously form at the cathode during the electrodeposition process and pose a challenge for the reliable application of electroplating methods to the fabrication of functional Re films. Defects due to hydrogen embrittlement or hydrogen outgassing during deposition are manifested as cracks in the final film, which would likely be detrimental to a device's performance. Our early work has shown that it is possible to overcome this challenge by electrodepositing rhenium from a solution containing an ultra-high concentration of lithium chloride.⁸ This type of solution is known as a water-in-salt electrolyte,^{9–13} and is able to suppress hydrogen evolution during electrodeposition at hydrogen overpotentials.

The crystal structure of rhenium films has been closely related to their superconductivity, with disordered samples exhibiting higher T_c than highly crystalline ones.^{14,15} Microelectronic devices often undergo thermal annealing or other thermal cycles during the fabrication processes. The stability of superconductivity against thermal treatment is, therefore, critical for device applications. This work characterizes rhenium thin films grown via electrodeposition from a water-in-salt electrolyte and evaluates the annealing conditions under which these films experience crystal grain growth, as well as the effect grain growth has on the T_c of the material. Attention is paid to impurities incorporated into the film while electroplating from this electrolyte. Electrochemical studies of Re electrodeposition from water-in-salt electrolytes are also provided, and the effect of the hydrophobic cation tetra-butyl ammonium (TBA) has been investigated to achieve further suppression of hydrogen evolution.

II. METHODS

All electrochemical studies and electrodeposition were performed in solutions made of 18.2 MΩ cm water, 25 mM ammonium perrhenate(VII) (99%), and 0.1M sulfuric acid (96%–98%). Water-in-salt electrolytes also contained 5M lithium chloride (98%) and tetrabutylammonium hydrogen sulfate (98%). All electrochemical work was performed in a 3-compartment cell with a platinum foil counter electrode separated from the cathode by a glass frit and a saturated calomel reference electrode (SCE) fixed in position through a Luggin capillary. All potentials reported in this work are with respect to the SCE. Electrochemical studies were performed on a 5 mm diameter Pt rotating disk electrode (RDE). A rotation rate of 400 RPM was maintained throughout all work to provide adequate agitation for any formed hydrogen bubbles to be rapidly swept away. All electrochemical studies were carried out at room temperature (20 °C).

Voltammetric sweeps were performed at a rate of 100 mV/s. A high scan rate was used in order to complete experiments before accumulation of hydrogen bubbles on the electrode became significant. Due to RDE rotation and the fast diffusion of protons, which make up the bulk of the measured reduction current, no transient effects were observed by comparing against slower scan rates. Therefore, it is assumed that cyclic voltammograms (CVs) approximate steady state behavior. Partial currents were measured by electroplating rhenium for 60 s, followed by immediate anodic stripping at 0.7 V in the same solution. The integrated stripping charge was used to calculate the amount of Re deposited using Faraday's law, assuming that the Re cathodically deposits and anodically strips from/to

the same oxidation state(+VII), which will be briefly discussed in Sec. III A. This plating time was suitably long to give a good signal-to-noise ratio in stripping charge measurements and to allow neglect of any substrate interactions such as nucleation. Electrodeposited samples were made using silicon coupons with gold strips as seed layers. These substrates were prepared by first thermally forming a 50 nm layer of SiO₂ onto a Si wafer. The wafer was then patterned using lithography to create a 1 mm by 10 mm strip connected to a 3 mm by 5 mm contact pad. A 10 nm layer of Ti followed by a 100 nm layer of Au was evaporated. The photoresist was lifted off, leaving the patterned metal films. These substrate coupons were mounted onto a chuck rotating in the same way as the RDE. Electrical connection was made through a front contact pin to the pad. After deposition, a 20 nm layer of Au was sputtered onto the deposits to provide protection against surface oxidation in ambient.

A potentiostat with a frequency analyzer was used for all electrochemical work. Solution resistance was determined through electrochemical impedance spectroscopy, wherein a sinusoidal potential was applied with an RMS amplitude of 10 mV and the frequency was sampled from 0.1 Hz to 100 kHz. The solution resistance was used to correct for ohmic voltage drop in results where indicated. Film thickness was measured using a stylus profilometer. Measurements spanned the entire width of the strip and were averaged over at least 3 points along the length of the strip. Sample resistance measurements were performed using a cryogenic physical property measurement system capable of reaching temperatures down to 1.8 K. A linear four-point probe method was used with contact made through aluminum wires wire-bonded to the samples. Current was held constant at 1 mA and probes were separated by approximately 2 mm. *Ex situ* x-ray diffraction (XRD) was performed using a diffractometer with a Co Kα x-ray source. *In situ* XRD was performed during annealing experiments using a theta-theta diffractometer with an x-ray Kα line from a Cu target with 40 kV at 30 mA, where the ambient atmosphere and temperature are precisely controlled. The temperature ramp rate was 1 °C/min, and two 10 s diffractogram snapshots were taken every 10 °C. No correction was made for the temperature increase during the snapshots, which was less than 0.2 °C. Impurity content was measured with time-of-flight secondary ion mass spectrometry (TOF-SIMS) equipped with a Bi cluster liquid metal ion source, which generated a pulsed 25 keV Bi₃⁺ primary ion beam and sampled over an area of 65 μm by 65 μm. The SIMS instrument is routinely used for the detection of a wide spectrum of elements, including the ones interested to this study. To obtain depth profiles, the sample was sputtered with a 3 keV Cs⁺ ion beam over an area larger than the SIMS measurement area. Depth profiles were obtained by alternating between sputtering for 2 s at a rate of 0.9 nm/s and SIMS analysis for 1 s. The sputtering rate was calibrated with AFM profilometer measurement over the final crater.

III. RESULTS AND DISCUSSION

A. Electrochemical behavior of rhenium deposition electrolytes

The use of water-in-salt electrolytes to reduce hydrogen evolution during the electrodeposition of rhenium has been documented in our previous publications.^{6,8} A decrease in proton reduction

current, achieved by limiting the proton diffusion rate, has been shown when high concentrations of LiCl of 5–10M are dissolved in solution.¹⁶ This effect alleviates hydrogen embrittlement in growing Re films and achieves the elimination of pinholes and cracks in thin film deposits. Here, a study is presented quantifying the effects that the addition of 5M LiCl has on the Re deposition rate and proton reduction rate in a Re plating electrolyte consisting of 25 mM NH_4ReO_4 and 0.1M H_2SO_4 . Figure 1(a) presents the cathodic sweep of CVs of the rhenium electrolyte both with 5M LiCl (green line) and without LiCl (red line). Potentials were corrected for ohmic drop prior to plotting. As the potential is swept away from an open-circuit value in the cathodic direction, the proton reduction reaction occurs with fast kinetics beginning at -0.28 V and -0.21 V vs SCE in the additive-free and 5M LiCl electrolytes, respectively. This shift in the onset potential of proton reduction is notable and indicates that protons, complexed as hydronium ions, are present in a different chemical state in the water-in-salt electrolyte. The positive direction of this shift indicates that the hydronium ions are more easily reduced to hydrogen gas. The H_2O to LiCl molar ratio in a 5M LiCl solution is 9.6,⁶ less than the amount necessary to completely fill the primary solvation sheaths of all Li^+ and Cl^- ions. Studies have demonstrated that Li^+ and Cl^- in concentrated solutions have water coordination numbers of 4.1 and 7.8, respectively.^{17,18} These electrolytes cannot be assumed to behave similarly to dilute electrolytes—every water molecule is expected to experience interactions with solute ions. In this case, the Lewis acidity of the Li^+ ions either in the solution or adsorbed on the electrode surface are believed to weaken the $\text{O}-\text{H}^+$ bonds in hydronium ions, promoting the acidity of hydronium and making proton reduction more thermodynamically favorable.

Although the thermodynamics and reaction kinetics of hydrogen evolution seem to be shifted favorably in the water-in-salt electrolyte, the CV experiments reveal a mass transport limitation of the proton reduction reaction which establishes a limiting current at -0.35 V, at which point the current does not significantly increase until water reduction begins at -1.4 V. Mass transport of protons to the electrode surface is limited in the presence of concentrated LiCl by the disruption of the extensive hydrogen-bonding network, which normally allows for fast proton diffusion in water through the Grotthuss mechanism.^{19,20} Due to this mass transport limitation, the current corresponding to hydrogen evolution is limited to 120 mA/cm^2 throughout the potential region, where Re deposition occurs. In the electrolyte without LiCl, no such limitation of hydrogen evolution occurs, so despite the less favorable reaction kinetics and thermodynamics, LiCl free electrolytes exhibit greater hydrogen evolution beyond -0.7 V.

Rhenium deposition begins at -0.53 V. Concerning this reaction, a stark difference is also observed between the traditional electrolyte and the water-in-salt electrolyte. The onset potential does not change, indicating that Re is present in the same chemical state in both solutions. However, the kinetics of the Re deposition reaction are much faster in the water-in-salt electrolyte. Re deposits over 6 times faster in the water-in-salt electrolyte at -0.8 V, where the total current, including hydrogen evolution, is, however, equal between the two solutions. In other words, this water-in-salt electrolyte can, therefore, achieve over an 80% reduction in hydrogen evolution during rhenium plating on a thickness basis.

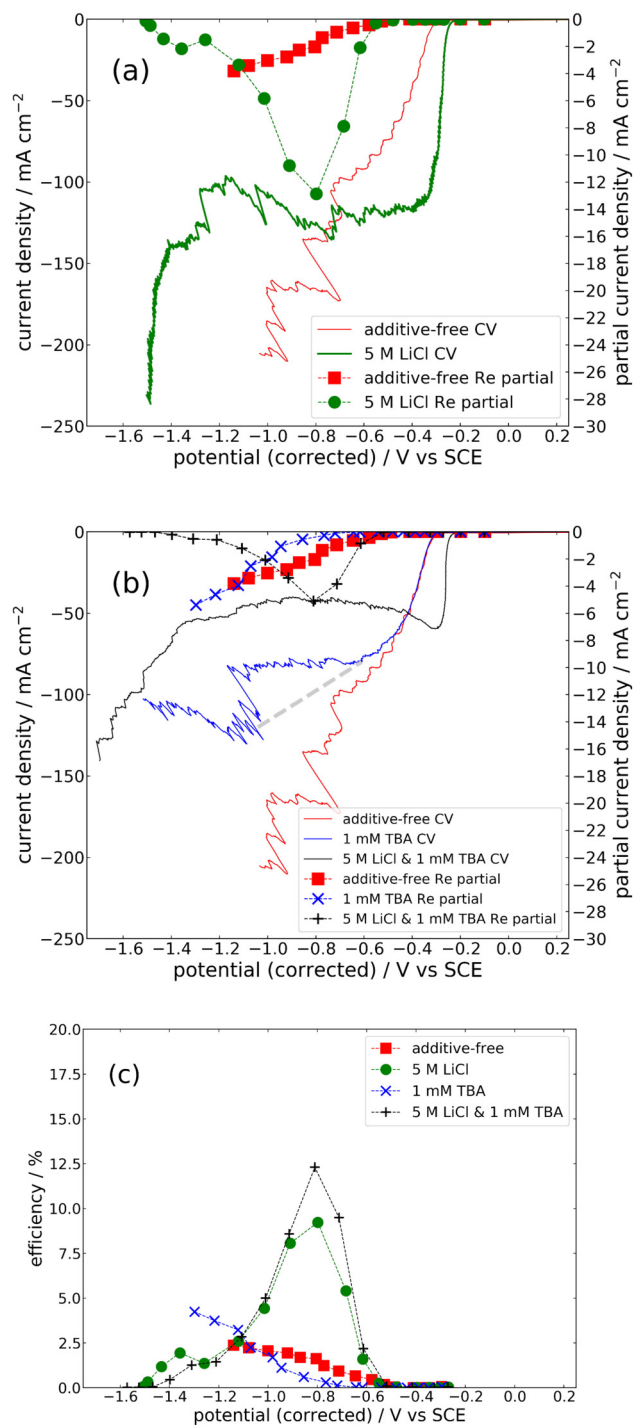


FIG. 1. (a) Cyclic voltammograms showing partial currents (dashed lines with markers) and total currents (solid lines) of rhenium deposition on a Pt RDE at 400 RPM with and without 5M LiCl; (b) effects of TBA on the CVs and partial currents of rhenium deposition; and (c) current efficiencies of rhenium deposition with various solution additives.

Partial currents are calculated based on an assumption that Re oxidizes to the same oxidation state (VII) from which it was initially reduced. If it were to have oxidized to a less positive state, the partial currents calculated would be an underapproximation. However, potentiostatic rhenium depositions on Au strip substrates used for fabricating samples for material characterization later in this study allow for a direct thickness measurement with a profilometer. By using Faraday's laws of electrolysis, the Re deposition partial current was calculated from the thickness and is exhibited in Figure S-1 in the [supplementary material](#), which is approximately equal to the values obtained from anodic stripping. From these calculations, it is confirmed that the stripping analysis method does not give a significant underapproximation of the partial current, suggesting that Re does oxidize primarily to the (VII) state.

It is interesting to note that in the presence of concentrated LiCl, there is a gradual reduction in the Re deposition rate once cathodic potentials are held below -0.8 V, and once the potential is held at -1.5 V or beyond, no Re deposit is found on the electrode. No such behavior is observed in the solution lacking LiCl. The phenomena resulting in decreased Re deposition at more negative potentials in LiCl containing solutions are not fully understood, but may include a number of causes. Our group has recently discovered that copper deposition in a similar water-in-salt electrolyte comes to a halt upon reaching the onset potential of water reduction,¹⁶ and has attributed this to the formation of insoluble and non-conducting lithium hydroxides on the cathode surface.²¹ Additionally, manganese electrodeposited from a deep eutectic solvent containing similarly a high chloride concentration forms a passivating layer at highly negative potentials.²² While this mechanism likely explains the halting of Re deposition we have observed at -1.5 V, it does not seem to adequately explain the gradual decrease in the Re deposition rate beginning at -0.8 V, as water reduction is not occurring here and so there should not be sufficient quantities of hydroxide near the cathode to form a passivating layer. Our group has also previously noted a similar behavior for Re deposition in the water-in-salt electrolyte, while the observation here confirms that the presence of concentrated LiCl is necessary for such a suppression effect to occur. The detailed mechanism is unknown, but a complexed alkali metal rhenium hydride^{23–26} intermediate species may be involved.

In the vein of further reducing hydrogen evolution during the electrodeposition of Re, the use of the hydrophobic cation TBA has been evaluated. TBA has been observed to adsorb onto negatively biased electrode surfaces and, due to its hydrophobic nature, block water molecules from subsequently accessing the surface.²¹ Upon the addition of 1 mM TBA to the Re plating solution, a decrease in both the total current and the Re partial current is observed during potential sweep experiments as shown in Fig. 1(b). Tetra-alkyl ammonium salts and other positively charged nitrogen-containing organic compounds have been used in the past as levelers in electroplating, where the surface blocking or suppression is typically ubiquitous regardless of the details of charge transfer reactions.²⁷ While the TBA cation suppresses the hydrogen evolution, it proportionally suppresses the Re deposition reaction. Upon first glance, it appears as though a proton reduction limiting current of 80 mA cm^{-2} is established at -0.61 V induced solely by the

blocking effects of 1 mM TBA. This behavior would be unexpected for an interface effect as proposed here. Further inspection reveals that the horizontal portion of the CV between -0.61 V and -1 V is likely not due to a limiting current, but rather is an artifact of hydrogen bubbles forming and effectively reducing the surface area of the working electrode. The jump to higher current density at -1.05 V results from such a bubble becoming displaced by the rotation. If the peak current measured at this point is used to interpolate a typical kinetics-controlled current-potential dependence, as shown by the dashed gray line in Fig. 1(b), it becomes clear that there is a potential dependent slow-down in the kinetics of the proton reduction reaction that becomes stronger as the electrode potential becomes more negative. This is consistent with the expectation that the TBA cation adsorbs more strongly to the electrode surface at more negative potentials.

Notably, in combining the hydrogen evolution suppressing effects of TBA with the proton mass transport limiting effects of LiCl, the result is up to an 80% decrease in total current vs the additive-free Re plating solution, with the decrease caused overwhelmingly by a reduction in hydrogen evolution current. As seen in Fig. 1(c), the maximum current efficiency attainable in a water-in-salt electrolyte is 3% (absolute percentage points) higher when TBA is utilized. Therefore, it becomes possible to deposit Re at an efficiency of over 12% in our electrolyte, a 5 \times improvement over the additive-free electrolyte.

B. Superconductivity and grain structure of electrodeposited rhenium

The T_c of superconducting films is critical for implementation in devices. Films with greater T_c values are generally favored as they exhibit superconductivity at more achievable temperatures. Films of varying thicknesses from 90 to 850 nm were cathodically electrodeposited from water-in-salt electrolytes. The resistive T_c of these films, seen in Fig. 2(a), ranged from 4 K to 5.6 K, with typical transition widths of 0.2 to 0.4 K. Although crystalline Re has a T_c of 1.7 K,^{14,28,29} electrodeposited Re has been found to have a T_c of up to 6 K when fabricated as stacked multilayers with Au,⁵ and we have achieved similar values for single Re layers, over a wide range of thicknesses, deposited from a water-in-salt electrolyte. We attribute the elevated T_c values to the highly disordered atomic structure of electrodeposited Re films. Indeed, an enhanced T_c up to 7 K has been reported for amorphous films of Re prepared using vapor-quenching⁷ or ion implantation.¹⁵ The superconductivity of a crystalline material can be related to the interaction between electrons and phonons, and, therefore, depends on the lattice structure. However, a well-defined lattice structure is absent in amorphous materials and the critical temperature not only differs from the crystalline material but also strongly depends on the number of unpaired electrons in the d-orbitals.⁷ The T_c 's of amorphous 5d transition metals show an oscillatory nature and, rhenium, which comprises the maximum number (five) of half-filled d-orbitals, relates to one of the highest T_c 's of its amorphous neighbors. Electrodeposition is a non-equilibrium process and, therefore, often deposits films with refined grains in a metastable, disordered fashion. The crystal nature of our films has been studied by XRD as presented in Fig. 3. Regardless of the thickness, the as-deposited

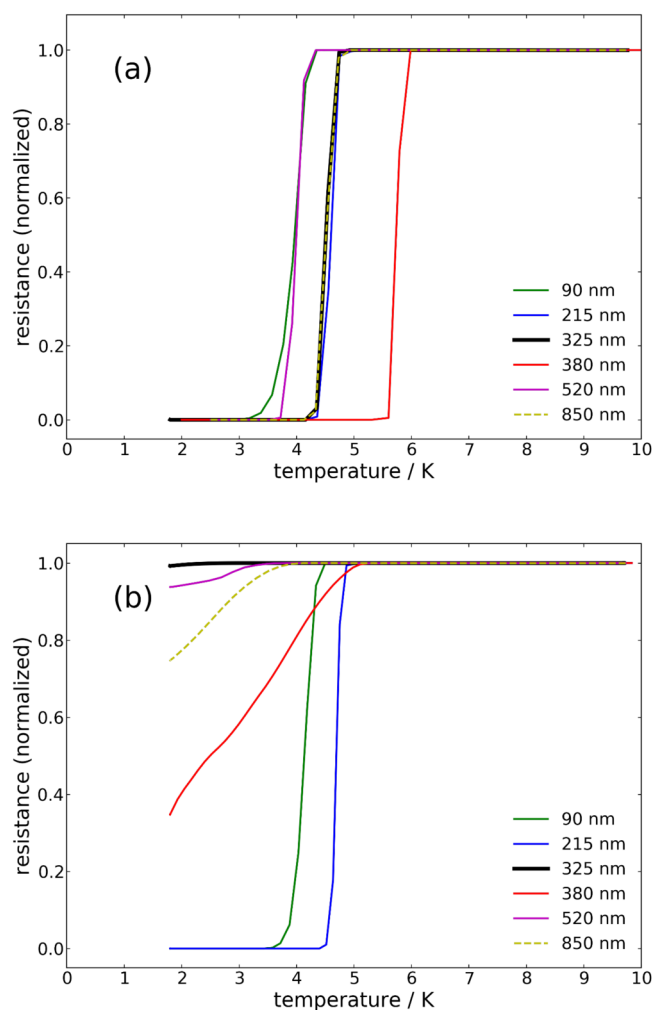


FIG. 2. Resistances of Re films (a) as-deposited from the water-in-salt electrolyte and (b) after annealing at 200–225 °C under vacuum.

films do not exhibit any XRD peaks corresponding to Re crystal structure. The peaks can be assigned to the crystal structure of Au from the seed and cap. This indicates that Re is present in our films in a nano-crystalline or amorphous state. No differences in the diffractograms were observed after several weeks, suggesting the Re thin films do not crystallize at room temperature.

To further elucidate any correlation between crystallinity and superconductivity, annealing was performed for 30 min in a vacuum furnace operated at 200 °C. It should be noted that an initial temperature overshoot of up to 25 °C was typically observed during the ramping, meaning that annealing temperatures briefly reached up to 225 °C before stabilizing to 200 °C. Reflections from the Au layer remained the same, consistent with the immiscibility between Au and Re at these temperatures.³⁰ The crystallization behavior of Re was highly dependent on the film thickness, as seen in Fig. 3. Films 325 nm thick and thicker experienced significant

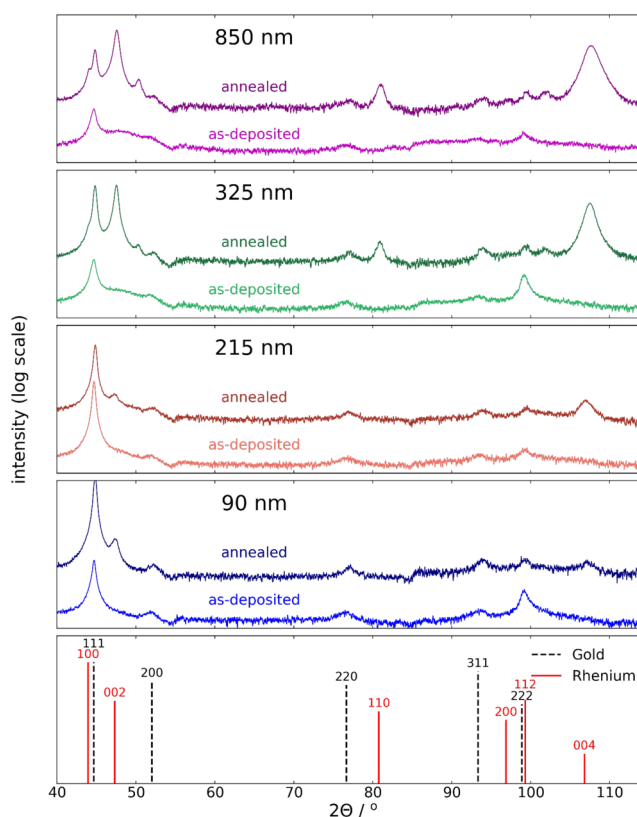


FIG. 3. X-ray diffractograms of selected Re films as-deposited and after vacuum annealing at 200 °C for 30 min. The bottom plot shows peak locations and relative intensities of a calculated x-ray diffractogram of an ideal Re powder sample, using a Co $K\alpha$ x-ray source.

grain growth in all directions. However, it is seen by comparing the relative peak intensities to those for a powder sample that the grain growth significantly favors the c direction. Scherrer's equation was used to determine the average crystallite size, accounting for instrumental line broadening of 0.3° and assuming a shape factor of 0.9. It should be noted here that although the absolute values of the grain size obtained from this method may suffer poor precision, it is chosen here to allow relative comparison between different growth directions and to show the effect of annealing on the grain structure. The 850 nm film has an average grain size in the c direction of 84 nm based on the (002) peak, however the grain size in the a direction is only 34 nm based on the (110) peak. The annealed 350 nm Re film had average grain sizes of 53 nm and 22 nm in the respective directions. The thinner films experienced very little grain growth. The little crystal structure observed in the annealed 90 and 215 nm films was exclusively in the c direction. Based on the (002) peak, average crystallite sizes grew to 14 nm in both films. No (110) peak was observed in these samples. This indicates that grain growth of Re films can be largely inhibited due to pinning by the adjacent metal layers if the Re layer is kept sufficiently thin. Similar behavior is well known for electrodeposited

copper, where films with thicknesses of 250 nm or less, or constrained within trenches of similar dimensions, are found to undergo significantly more sluggish crystal grain growth during annealing.^{31,32} Upon measuring the T_c of the annealed Re films, presented in Fig. 2(b), it was confirmed that atomic structure was highly correlated to superconductivity. After annealing, the films that were 325 nm or thicker, which had been demonstrated by XRD to have undergone significant grain growth, no longer exhibited superconductivity above 1.8 K, the minimum temperature our measurements were capable of achieving. This is consistent with the knowledge that the T_c enhancement was due to the lack of crystalline periodicity in amorphous structure.³³ Such an enhancement, therefore, vanishes upon the crystallization at elevated temperatures. In contrast, the 90 and 215 nm films, which remained highly disordered upon annealing, exhibited no decrease in the T_c upon annealing, indicating that the disordered atomic structure is responsible for the elevated T_c in electrodeposited Re. Furthermore, this may indicate an anisotropic impact of the crystallization on superconductivity. The c direction grain growth may not impede superconductivity; but grain growth in the a and b directions significantly reduces T_c . The beneficial effect of maintaining film thicknesses less than some critical value between 215 and 325 nm points to a possible strategy of using layers of thin electrodeposited Re as a means to stabilize the disordered atomic structure of superconducting Re lines. This may also point to using multilayer structures rather than thick Re layers to allow high current without sacrificing the amorphous structure stability. Current densities comparable to that of superconducting Nb films are typically observed in these films with similar temperature-dependent behavior.⁵

To ensure that the elevated T_c is not due to an effect of the interface between the Au and Re layers, a sample was deposited onto the same strip patterned substrate, but with a Pd seed as opposed to Au, with no protective Au layer deposited. Figure 4 shows that this sample, having a 440 nm layer of Re, and a 680 nm sample deposited in the same batch on the Au substrate as a control, have identical T_c

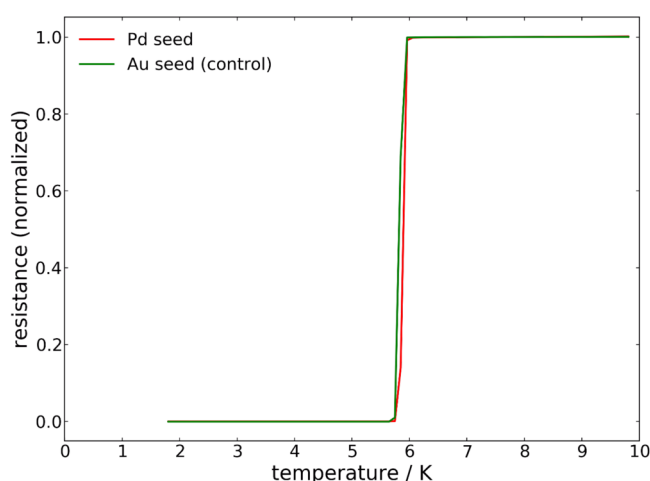


FIG. 4. Resistances of Re films deposited on Au or Pd seed layers.

values. It can, therefore, be concluded that the superconductivity of our films arises from the bulk of the Re deposit, and is not affected by the interface with other metal layers.

The temperature at which crystallization of Re occurs was determined more precisely by taking *in situ* XRD measurements during annealing as the temperature was slowly ramped up at a rate of 1 °C/min. A dwell time of 20 s was used for every 10 °C, when a diffraction pattern was captured. The effects of the annealing ambient were also studied. The resulting diffractograms are plotted in Fig. 5. A narrow 2θ range was selected that covers only the Au (111) peak and the Re(002) peak, as these peaks appear in annealed samples of every thickness previously studied. In both the 193 and 367 nm films, which were annealed in 100% N₂ [Figs. 5(b) and 5(c), respectively], the Re(002) peak does not emerge until the temperature reaches 220 °C. A small peak of constant height observed across all temperatures in Figs. 5(b) and 5(c), at different 2θ locations. It was, however, not observed in any of the other diffraction patterns, and cannot be assigned to the rhenium lattice, the substrate, or the stage holder. It is, therefore, believed to result from surface contamination, possibly occurring during shipping between sample preparation and *in situ* XRD measurements. The films annealed with 4% H₂ (Figs. 5(a) and 5(d), 88 and 566 nm, respectively) had emergent Re(002) peaks much earlier at 190 °C. The sample was clamped on a thermally controlled stage during the XRD analysis with the gas flow across the chamber. While H₂ does have a slightly higher thermal conductivity than N₂, this difference is believed to be insignificant with the small fraction of H₂, as compared to the large temperature difference measured for crystallization. Furthermore, this small difference would have caused further overestimation of the crystallization temperature of 190 °C in H₂ ambient. Therefore, this difference in grain growth behavior may be attributable to hydrogen gas acting to reduce oxides or chlorides present along the grain boundaries. For example, the reactions between Re₂O₃ and H₂ or between ReCl₃ and H₂ are both expected to be thermodynamically spontaneous at these elevated temperatures, resulting in Re metal and H₂O or HCl.³⁴ If oxides are present along the grain boundaries, they could pin the grains and inhibit growth until higher temperatures. Hydrogen may, however, act to reduce these oxides, allowing the crystal grains to grow at lower temperatures.

C. Impurity analysis of water-in-salt deposited Re

When electrodepositing metals from a high-chloride solution, the incorporation of chloride into the deposit is often inevitable due to the ion's strong affinity for adsorption onto metal surfaces. In some cases, chloride and other impurities incorporated into metal films have an inhibiting effect on crystal grain growth within the film.³² As previously discussed, inhibition of grain growth in Re films is beneficial for superconductor applications where maintaining a high T_c is desired. On the other hand, alkali metal contamination is a major concern in semiconductor devices and fabrication facilities because of their high diffusivity and reactivity with Si.³⁵ Although the use of water-in-salt electrolyte did not affect the T_c of our as-deposited films when compared to films deposited from a traditional Re electrolyte, the impurity content was studied to determine which impurities were incorporated into

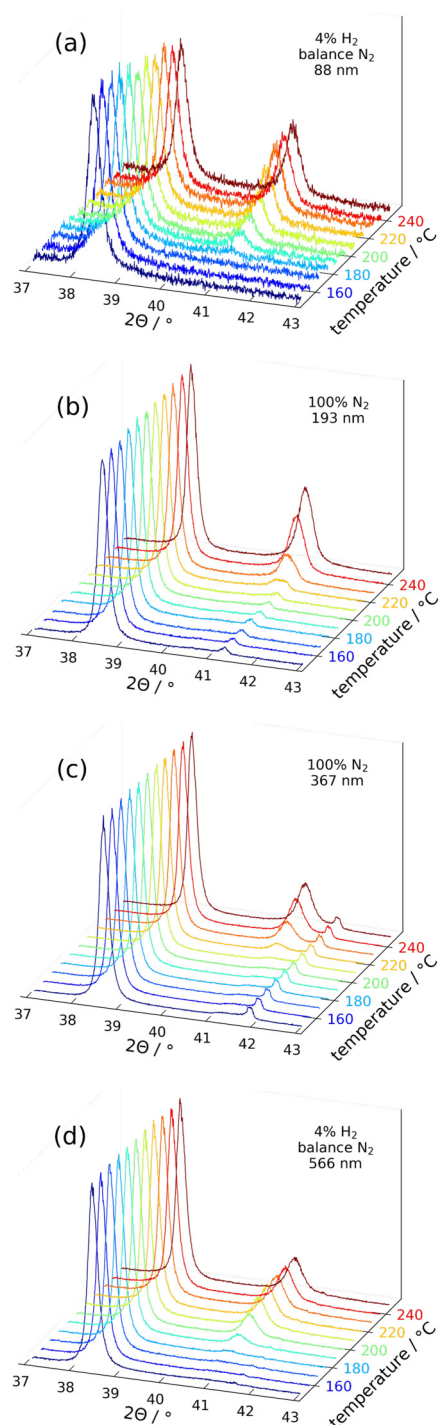


FIG. 5. X-ray diffractograms taken *in situ* during annealing of Re films of (a) 88, (b) 193, (c) 367, and (d) 566 nm in [(a) and (d)] 4% H_2 with 96% N_2 and [(b) and (c)] 100% N_2 , plotted on a linear scale. Peaks at 38.2° correspond to the Au (111) lattice, and peaks at 40.5° correspond to the Re (002) lattice. The higher angle peak in (c) is believed to result from surface contamination.

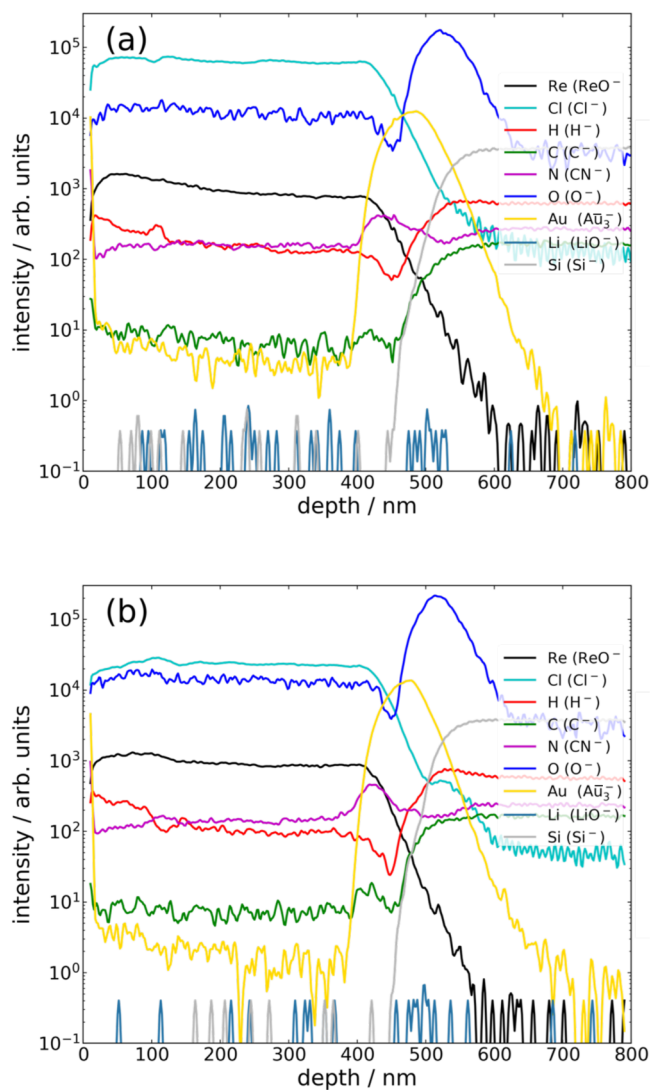


FIG. 6. SIMS depth profiles showing impurity content of Re films electrodeposited from the water-in-salt electrolyte (a) as-deposited and (b) annealed for 30 min at 200°C . Lower depth values below 500 nm correspond to the Re film, and higher depth values the Au seed/Si substrate.

the deposit and how annealing affects them. Depth profiling SIMS was performed on samples containing approximately 500 nm thick Re films deposited from the water-in-salt electrolyte, both before and after annealing at 200°C for 30 min. Results, shown in Fig. 6, have been scaled using the intensity of silicon in the silicon layer as a reference to avoid variation of the detector yield across samples. While not quantitative, these measurements provide a good understanding of the changes in impurity content during the annealing and crystallization process. SIMS indicated the presence of Cl, O, H, and N within the deposited Re layer, with a less significant amount of C. Upon annealing at 200°C for 30 min in a N_2

TABLE I. Change in SIMS detection intensity of impurity elements in Re upon annealing.

Element	Change upon annealing
Carbon	Negligible
Chlorine	−63%
Hydrogen	−28%
Nitrogen	−13%
Oxygen	+16%

atmosphere, no significant change was observed in most impurities such as C, N, O, as summarized in Table I. However, the chlorine content was significantly reduced by 63%. The second most pronounced change was a decrease in hydrogen content, but merely by 28%. The mechanism of chlorine decrease is so far unclear, and further study would be needed to confirm the change and understand the redistribution of these impurities upon annealing. On the other hand, the oxygen content was found to very slightly increase during annealing. If this small increase is confirmed to be real, it may reflect the slight contamination of the ambient during annealing.

Lithium was not detected above measurement noise levels in either sample, suggesting the incorporation of alkali metal in Re deposited from this water-in-salt electrolyte is negligible. This is a bit surprising since a very high current density of beyond 100 mA/cm² was used for Re deposition. Germanium thin film electrodeposited from a propanediol electrolyte using chloride salt³⁶ at 400 mA/cm² incorporated a very high level of potassium and sodium even though they were only introduced in trace amount through the molecular sieve used to dry the solvent (Figure S-2 in the supplementary material). However, the SIMS instrument has been routinely used for the detection of a variety of elements in various materials, including lithium, and this absence of Li may suggest some intrinsically different behaviors in terms of impurity incorporation between organic solvent and aqueous electrolyte—even if the latter has an extremely high concentration of solute salts. Organic molecules are believed to form complexed structures with cationic species including Li and results in the co-incorporation of the latter with the organics adsorbates. This appears not to take place in the water-in-salt aqueous electrolytes.

IV. CONCLUSION

The use of water-in-salt electrolytes for electrodepositing Re has been shown to reduce simultaneous hydrogen evolution, enabling deposition at higher rates and current efficiencies. The additive tetrabutylammonium further reduces the hydrogen evolution rate during Re electrodeposition. However, it also suppresses the Re deposition rate. A variety of thicknesses of Re thin films have been deposited, which exhibit superconductivity up to 5.6 K. This elevated T_c value is attributed to the disordered atomic structure of the deposits achieved by electrodeposition. While grain growth deteriorates the T_c of Re films, such a grain growth during annealing can be inhibited if the Re layers are sufficiently thin. An anisotropic effect of crystallization has been observed, where

T_c deterioration occurs upon grain growth in a and b directions, but not in c direction. Hydrogen present in the annealing atmosphere accelerates grain growth, allowing crystallization to occur at reduced temperatures. Chlorine and hydrogen are incorporated as impurities into Re films during deposition; however, their contents in films are significantly reduced by annealing.

SUPPLEMENTARY MATERIAL

See the supplementary material for rhenium deposition partial current densities and SIMS depth profile of impurities typically incorporated during electrodeposition with an organic solvent.

ACKNOWLEDGMENTS

Q.H. acknowledges support from the CAREER program of the National Science Foundation through Grant No. CMMI-1941820 and the Research grant Council at the University of Alabama (UA) through a seed grant, No. RG-14741. The mechanical shop, glass Shop, central analytical facility, and microfabrication facility at UA are gratefully acknowledged for making substrates and experimental parts, and for instrumental access for characterizations. D.P.P. acknowledges support from IARPA through Grant No. 16002-D2017-1706230008 and the NIST quantum initiative for this work as well as helpful discussions with Donald David at CIRES. Dr. Heng-Yong Nie at the University of Western Ontario is acknowledged for SIMS analysis and result discussion.

REFERENCES

- Ozeryansky, "Method of production for multifilament niobium-tin superconductors," U.S. patent 5,127,149 (1992).
- Adelmann, L. G. Wen, A. Peter, Y. K. Siew, K. Croes, J. Swerts, M. Popovici, K. Sankaran, G. Pourtois, S. Van Elshocht, J. Bömmels, and Z. Tokei, "Alternative metals for advanced interconnects," in *Proc. IEEE International Interconnect Technology Conference, September 2014*, p. 173.
- Ghasemi and Z. Valefi, "Electrodeposition of rhenium-base layer as a diffusion barrier between the NiCoCrAlY coating and a Ni-based superalloy," *J. Alloys Compd.* **732**, 470 (2018).
- S.-Y. Chang, L.-P. Liang, L.-C. Kao, and C.-F. Lin, "Electroless- and electroplating of Cu(Re) alloy films for self-forming ultrathin Re diffusion barrier," *J. Electrochem. Soc.* **162**(3), D96 (2015).
- P. Pappas, D. E. David, R. E. Lake, M. Bal, R. B. Goldfarb, D. A. Hite, E. Kim, H. S. Ku, J. L. Long, C. R. H. McRae, L. D. Pappas, A. Roshko, J. G. Wen, B. L. T. Plourde, I. Arslan, and X. Wu, "Enhanced superconducting transition temperature in electroplated rhenium," *Appl. Phys. Lett.* **112**(18), 182601 (2018).
- Huang and Y. Hu, "Electrodeposition of superconducting rhenium with water-in-salt electrolyte," *J. Electrochem. Soc.* **165**(16), D796 (2018).
- M. M. Collver and R. H. Hammond, "Superconductivity in" amorphous" transition-metal alloy films," *Phys. Rev. Lett.* **30**(3), 92 (1973).
- Huang and T. W. Lyons, "Electrodeposition of rhenium with suppressed hydrogen evolution from water-in-salt electrolyte," *Electrochem. Commun.* **93**, 53 (2018).
- Dubouis, P. Lemaire, B. Mirvaux, E. Salager, M. Deschamps, and A. Grimaud, "The role of the hydrogen evolution reaction in the solid-electrolyte interphase formation mechanism for "water-in-salt" electrolytes," *Energy Environ. Sci.* **11**(12), 3491 (2018).
- Bin, F. Wang, A. G. Tamirat, L. Suo, Y. Wang, C. Wang, and Y. Xia, "Progress in aqueous rechargeable sodium-ion batteries," *Adv. Energy Mater.* **8**(17), 1703008 (2018).

- ¹¹R.-S. Kühnel, D. Reber, A. Remhof, R. Figi, D. Bleiner, and C. Battaglia, "Water-in-salt" electrolytes enable the use of cost-effective aluminum current collectors for aqueous high-voltage batteries," *Chem. Commun.* **52**(68), 10435 (2016).
- ¹²L. Suo, O. Borodin, T. Gao, M. Olguin, J. Ho, X. Fan, C. Luo, C. Wang, and K. Xu, "Water-in-salt" electrolyte enables high-voltage aqueous lithium-ion chemistries," *Science* **350**(6263), 938 (2015).
- ¹³L. Suo, Y.-S. Hu, H. Li, M. Armand, and L. Chen, "A new class of solvent-in-salt electrolyte for high-energy rechargeable metallic lithium batteries," *Nat. Commun.* **4**, 1481 (2013).
- ¹⁴J. K. Hulm and B. B. Goodman, "Superconducting properties of rhenium, ruthenium, and osmium," *Phys. Rev.* **106**(4), 659 (1957).
- ¹⁵A. U. Haq and O. Meyer, "Superconducting and electrical properties of rhenium nitride and amorphous rhenium prepared by ion implantation," *J. Low Temp. Phys.* **50**(1), 123 (1983).
- ¹⁶S. De, J. White, T. Brusuelas, C. Patton, A. Koh, and Q. Huang, "Electrochemical behavior of protons and cupric ions in water in salt electrolytes," *Electrochim. Acta* **338**, 135852 (2020).
- ¹⁷S. Bouazizi, S. Nasr, N. Jaidane, and M.-C. Bellissent-Funel, "Local order in aqueous NaCl solutions and pure water: X-ray scattering and molecular dynamics simulations study," *J. Phys. Chem. B* **110**(46), 23515 (2006).
- ¹⁸T. Yamaguchi, H. Ohzono, M. Yamagami, K. Yamanaka, K. Yoshida, and H. Wakita, "Ion hydration in aqueous solutions of lithium chloride, nickel chloride, and caesium chloride in ambient to supercritical water," *J. Mol. Liq.* **153**, 2 (2010).
- ¹⁹Q. Sun, "Raman spectroscopic study of the effects of dissolved NaCl on water structure," *Vib. Spectrosc.* **62**, 110 (2012).
- ²⁰C. J. T. de Grotthuss, "Mémoire sur la décomposition de l'eau et des corps qu'elle tient en dissolution à l'aide de l'électricité galvanique," *Ann. Chim.* **58**, 54–74 (1806).
- ²¹N. Dubouis, A. Serva, E. Salager, M. Deschamps, M. Salanne, and A. Grimaud, "The fate of water at the electrochemical interfaces: Electrochemical behavior of free water versus coordinating water," *J. Phys. Chem. Lett.* **9**(23), 6683 (2018).
- ²²W. D. Sides and Q. Huang, "Electrodeposition of manganese thin films on a rotating disk electrode from choline chloride/urea based ionic liquids," *Electrochim. Acta* **266**, 185 (2018).
- ²³J. E. Fergusson, "Recent advances in the coordination chemistry of rhenium," *Coord. Chem. Rev.* **1**(4), 459 (1966).
- ²⁴S. C. Abrahams, A. P. Ginsberg, and K. Knox, "Transition metal-hydrogen compounds. II. The crystal and molecular structure of potassium rhenium hydride, K_2ReH_9 ," *Inorg. Chem.* **3**(4), 558 (1964).
- ²⁵A. Woolf, "An outline of rhenium chemistry, quarterly reviews," *Chem. Soc.* **15**(3), 372 (1961).
- ²⁶J. W. Cobble, "On the structure of the rhenide ion," *J. Phys. Chem.* **61**(6), 727 (1957).
- ²⁷W. Wang, H. Hua, L. Yin, and Y. He, "Influence of the hydrophobic groups on quaternary ammonium additives for copper electrodeposition," *J. Electrochem. Soc.* **161**, D651 (2014).
- ²⁸J. G. Daunt and T. S. Smith, "Superconductivity of rhenium," *Phys. Rev.* **88**(2), 309 (1952).
- ²⁹J. Eisenstein, "Superconducting elements," *Rev. Mod. Phys.* **26**(3), 277 (1954).
- ³⁰P. Subramanian, D. Laughlin, and T. Massalski, *Binary Alloy Phase Diagrams* (ASM Handbooks Online, 1990).
- ³¹J. M. E. Harper, C. Cabral Jr., P. C. Andricacos, L. Gignac, I. C. Noyan, K. P. Rodbell, and C. K. Hu, "Mechanisms for microstructure evolution in electroplated copper thin films near room temperature," *J. Appl. Phys.* **86**(5), 2516 (1999).
- ³²J. Reid, "Damascene copper electroplating," in *Handbook of Semiconductor Manufacturing Technology*, edited by R. Doering and Y. Nishi (CRC Press, Boca Raton, FL, 2008).
- ³³G. Bergmann, "Amorphous metals and their superconductivity," *Phys. Rep.* **27**(4), 159 (1976).
- ³⁴I. Barin and G. Platzki, *Thermochemical Data of Pure Substances*, 3rd ed. (VCH Verlagsgesellschaft mbH, Weinheim, Germany, 1995).
- ³⁵L. Švob, "Solubility and diffusion coefficient of sodium and potassium in silicon," *Solid-State Electron.* **10**(10), 991 (1967).
- ³⁶Q. Huang, S. W. Bedell, K. L. Saenger, M. Copel, H. Deligianni, and L. T. Romankiw, "Single-crystalline germanium thin films by electrodeposition and solid-phase epitaxy," *Electrochim. Solid-State Lett.* **10**(11), D124 (2007).